Hybrid rocket engines simulation approach and its validation

Bartosz Hyży*[†], Michał Krajewski*, Michał Kret*, Szymon Krupa*, Piotr Łyżwa*, Remigiusz Michał, Michał Tomporowski* and Mateusz Sochacki**

* Students' Space Association, Faculty of Power and Aeronautical Engineering, Warsaw University of Technology ul. Nowowiejska 21/25, 00-665 Warsaw, Poland

** Division of Automation and Aeronautical Systems, Faculty of Power and Aeronautical Engineering, Warsaw University of Technology
ul. Nowowiejska 24, 00-665 Warsaw, Poland

bartosz.hyzy.stud@pw.edu.pl †Corresponding Author

Abstract

Hybrid rocket engines combine advantages of liquid and solid propulsion, offering simplicity, safety, and eco-friendly propellants. Their design includes separation of fuel and oxidiser, enhancing safety. The Rocketry Division of the Students' Space Association at Warsaw University of Technology, experienced in solid rocket motors development, began developing hybrids to enter global competitions. This led to development of hybrid rocket engines using nitrous oxide as oxidiser, culminating in Aurora 8 kN engine. However, its double-phase nature complicates simulation. This paper describes simulation methods using MATLAB-based RPAT programme, detailing physical models for oxidiser flow and combustion, validated with static fire test data.

1. Introduction

Hybrid rocket engines introduce a high level of operational safety, by providing separation of fuel and oxidiser in terms of both storage location and state of aggregation. This includes the impossibility of a situation in which whole propellant used in the system starts to react spontaneously within a given volume. This fact, as well as the possibility of using environmentally friendly propellants in this type of propulsion system, while maintaining satisfactory performance increases popularity of this propulsion type nowadays [1]. Finally, the overall simplicity of construction makes hybrid engines a particularly interesting technology to develop, however subsystems designs are usually more sophisticated (especially hydraulic systems).

A particular difficulty at the design stage of a hybrid engine, however, is that it is difficult to determine a priori the value of the linear burn rate of the fuel. This is a critical quantity in terms of the performance obtained during engine operation, as it affects the effective value of the oxidiser/fuel mass flow rate ratio obtained, which in turn determines the thermodynamic characteristics of the products and thus, among other things, the specific impulse of the engine (see Figure 1). The difficulty of determining the instantaneous value of the linear burn rate of the fuel is due to the complexity of the combustion process mentioned above (described in more detail in Chapter 3) and its sensitivity to the nature of the flow of oxidiser and combustion products along the fuel grain channel. This fact, combined with the wide range of hybrid engine combustion chamber configurations currently under development [2-6], and the wide spectrum of propellants used, leads to ambiguity regarding the selection of the correct combustion model. To address this problem, this article attempts to identify a combustion law model of the fuel that allows an accurate representation of its burn rate. For this purpose, a literature review will be carried out with the aim of identifying a number of promising combustion models, which will then be validated using Students' Space Association (SKA, Polish: Studenckie Koło Astronautyczne) Rocket Propulsion Analysis Tool (RPAT) and experimental data obtained during the static fire test of the Aurora hybrid engine developed within SKA for Twardowsky 2 rocket propulsion.

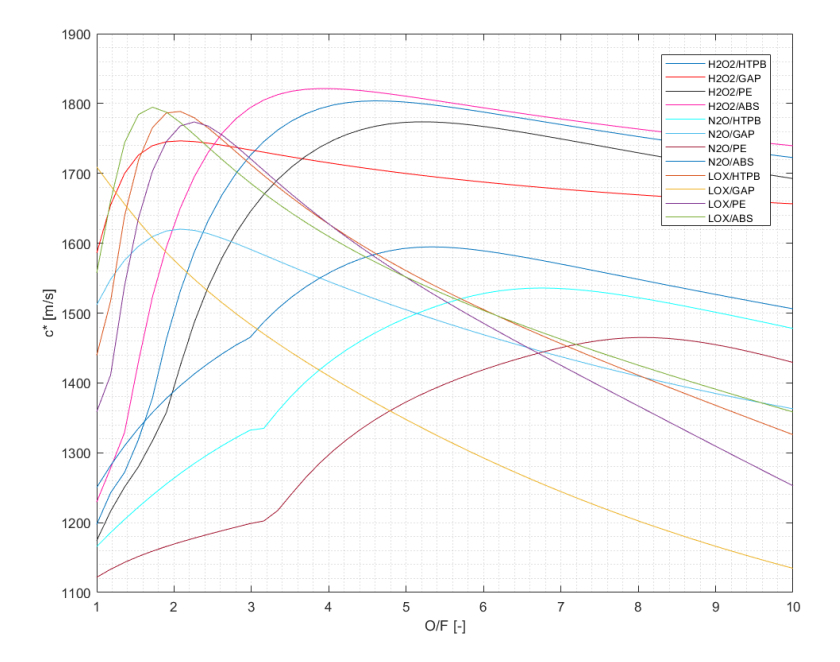


Figure 1 Comparison of characteristic velocity value for several hybrid propellant combinations. Presented data has been obtained using NASA CEA software [7]

2. Rocket motors simulation programme

The simulation of hybrid engines in the Association is primarily done utilising the in-house developed RPAT – Rocket Propulsion Analysis Tool programme, which enables the user to simulate the burn of grain in the thrust chamber and the changes of the oxidiser parameters in the tank (see Figure 2). The programme and its validation have been described in detail in [8]. Figure 3 presents RPAT graphical user interface.

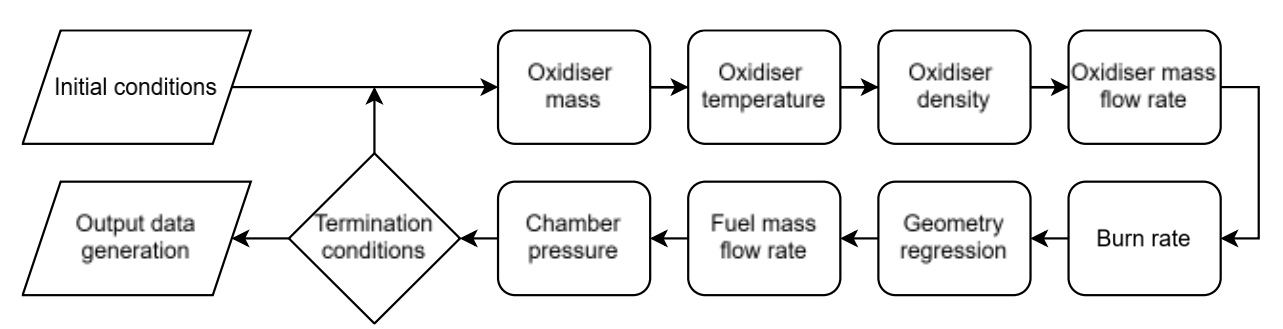


Figure 2 Block diagram describing the execution of RPAT programme

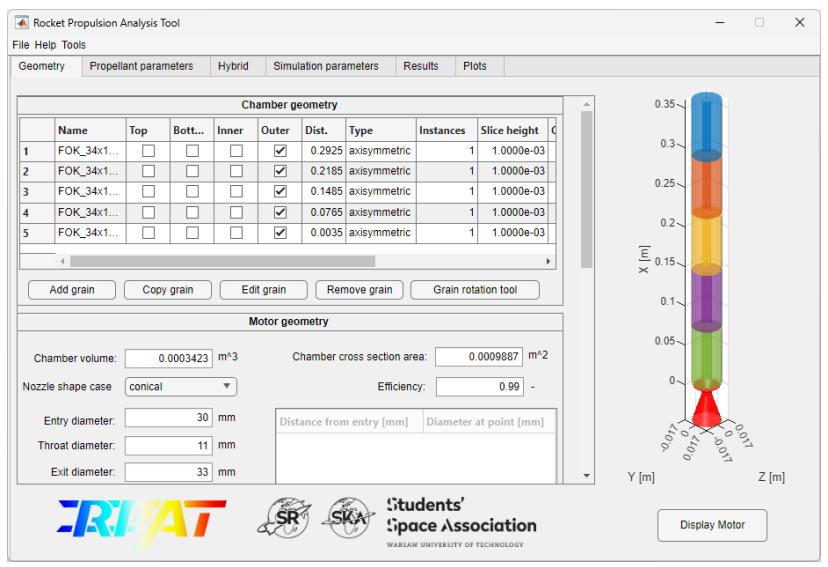


Figure 3 RPAT graphical user interface

The regression of the propellant grain is simulated using 2D or 3D methods. In 2D methods the grain is divided into slices along the grain's axis. Each slice is assumed to be described solely by its two-dimensional cross-section and its thickness. The grain regression is achieved by the translation of the grain's cross-section points along calculated burn rate vectors. Moreover, the top and bottom slices' thicknesses is also changed. The resulting change in volume and burn area of each slice is then used to calculate the changes in mass flow, chamber pressure, as well as other parameters. The 3D methods utilise the full 3D triangular mesh of the grain geometry and simulate the change of position of each vertex in every direction. Additionally, if the geometry of the grain exhibits certain type of symmetry such as axial symmetry or periodicity, only a portion of the geometry is actually modelled to reduce the computational time.

The oxidiser tank emptying process is simulated utilising two submodels of oxidiser discharge, according to the Dyer model [9]. The Single Phase Incompressible (SPI) model neglects the existence of gas phase in the fluid and assumes its incompressibility. The Homogeneous Equilibrium Model (HEM) assumes that phases co-exist in the hydraulic feed system in constant thermodynamic equilibrium. However, due to simplifying assumptions in each of the methods, the SPI overestimates and HEM underestimates the actual double phase mass flow rate. Due to this, to obtain the results closer to experimental values, the weighted average of the two values is taken:

$$\dot{m}_{SPI} = C_d A_{\text{injector}} \sqrt{2\rho_t (p_t - p_{ch})}$$
 (1)

$$\dot{m}_{HEM} = C_d A_{\rm injector} \rho_t \sqrt{2(h_t - h_{ch})}$$
 (2)

$$\dot{m}_{SPI} = C_d A_{\text{injector}} \sqrt{2\rho_t (p_t - p_{ch})}$$

$$\dot{m}_{HEM} = C_d A_{\text{injector}} \rho_t \sqrt{2(h_t - h_{ch})}$$

$$\dot{m}_{OX} = \frac{\chi \dot{m}_{SPI} + \dot{m}_{HEM}}{1 + \chi}$$
(3)

Where \dot{m}_{SPI} is mass flow rate calculated using SPI model, \dot{m}_{HEM} is mass flow rate determined using HEM model, C_d is oxidiser flow discharge coefficient, A_{injector} is total cross-sectional area of injection holes, ρ_t is density of oxidiser stored in tank, p_t is oxidiser tank pressure, p_{ch} is combustion chamber pressure, h_t is oxidiser specific enthalpy in tank conditions, and h_{ch} is oxidiser specific enthalpy in combustion chamber conditions. The double-phase coefficient χ is assumed as equal to 1, which corresponds to a situation in which the residence time of the oxidiser in the tight spaces of the oxidiser feeding system is close to its bubble growth time. This simplification still allows for obtaining accurate results for self-pressurising systems, as has been presented in [8]. During the work of the engine, four distinct mass flows control its performance. The oxidiser mass flow is given by equation (3). The mass flow rate from fuel grain m_f , mass flow rate due to gas decompression in the volume freed by burned fuel \dot{m}_w and the mass flow exiting the chamber through nozzle \dot{m}_d are given by:

$$\dot{m}_f = \rho_f A_b \dot{r} \tag{4}$$

$$\dot{m}_f = \rho_f A_b \dot{r} \tag{4}$$

$$\dot{m}_w = \frac{p_{ch} \frac{dV}{dt}}{RT_c}$$

$$\dot{m}_d = p_{ch} A_{th} \sqrt{\frac{\kappa}{RT_c}} \left(\frac{\kappa + 1}{2}\right)^{-\frac{\kappa + 1}{2(\kappa - 1)}} \tag{6}$$

Where ρ_f is the fuel density, A_b is the fuel grain burn area, \dot{r} is the fuel grain burn rate, $\frac{dV}{dt}$ is the time derivative of free volume in combustion chamber, R is the specific gas constant, T_c is the combustion products temperature, A_{th} is the nozzle throat area and κ is the specific heat ratio of combustion products. The generated pressure change, used alongside oxidiser mass flow in the fuel combustion calculations, is then:

$$\frac{dp}{dt} = \frac{RT_c}{V_{\text{free}}} (\dot{m}_f + \dot{m}_{OX} - \dot{m}_d - \dot{m}_w) \tag{7}$$

Where V_{free} is free combustion chamber volume. Apart from the physical calculations, the program allows for broad modification of parameters and the in-depth analysis of results. The tools available for the program include grain rotation tool, surface inhibition selection tool, 3D grain STL generator and graphical user interface. As an example of program capabilities, the simulation results of Association's newest hybrid engine Aurora are shown in Figure 4. The engine static fire test data will be used in later sections for the purpose of validation.

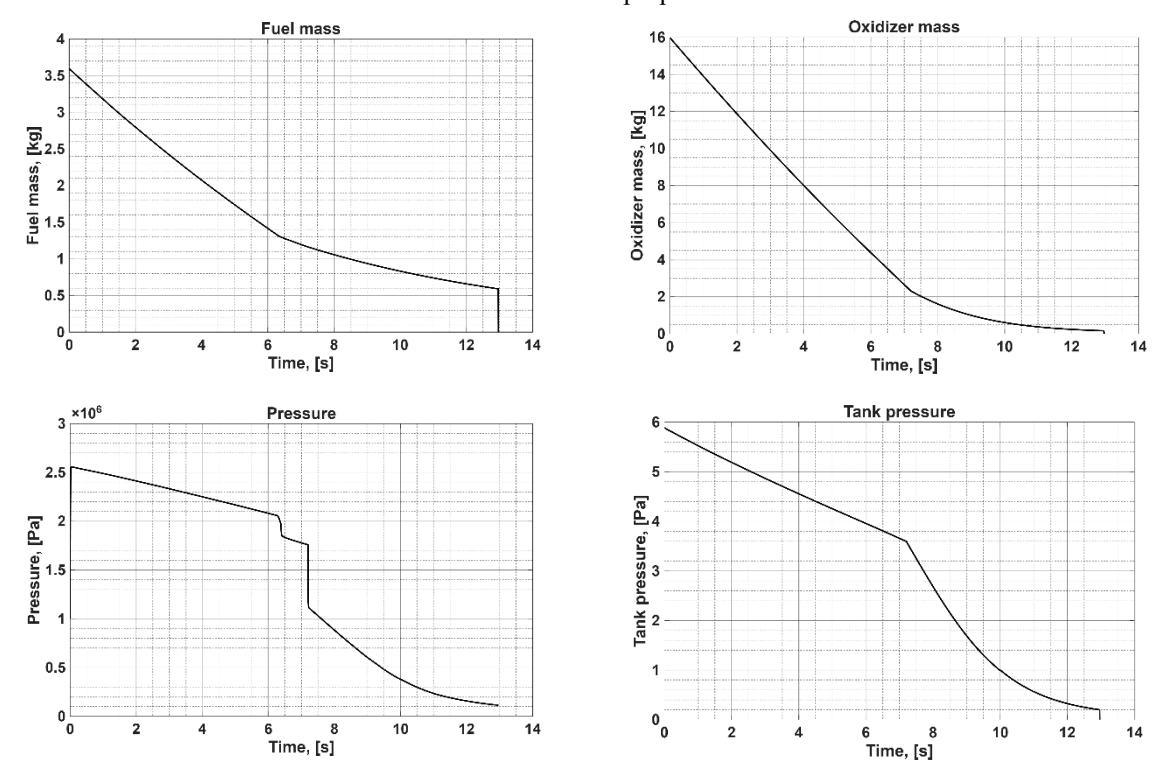


Figure 4 Plots visualizing the operation of hybrid engine Aurora with showerhead injector

Although RPAT has proven its effectiveness and accuracy over the years of development, currently only the 2D burn model is fully implemented. Dividing the grain into slices has proven to be effective in the case of most of the geometries, however as the burn vector is oriented in the plane of the grain cross-section, this method has its limitations. The first drawback of this method is its inability to start the burn of the uncovered surface in the case of the sudden step in the channel (see Figure 5). The second comes from the approximation error. The slice boundaries are parallel to the axis of the engine. Due to that, in the case of conical channel, the burn vector that should be oriented perpendicular to the surface, is not, which can produce substantial result discrepancies (see Figure 5). To alleviate these problems, the 3D models are in development, with axisymmetric one already implemented.

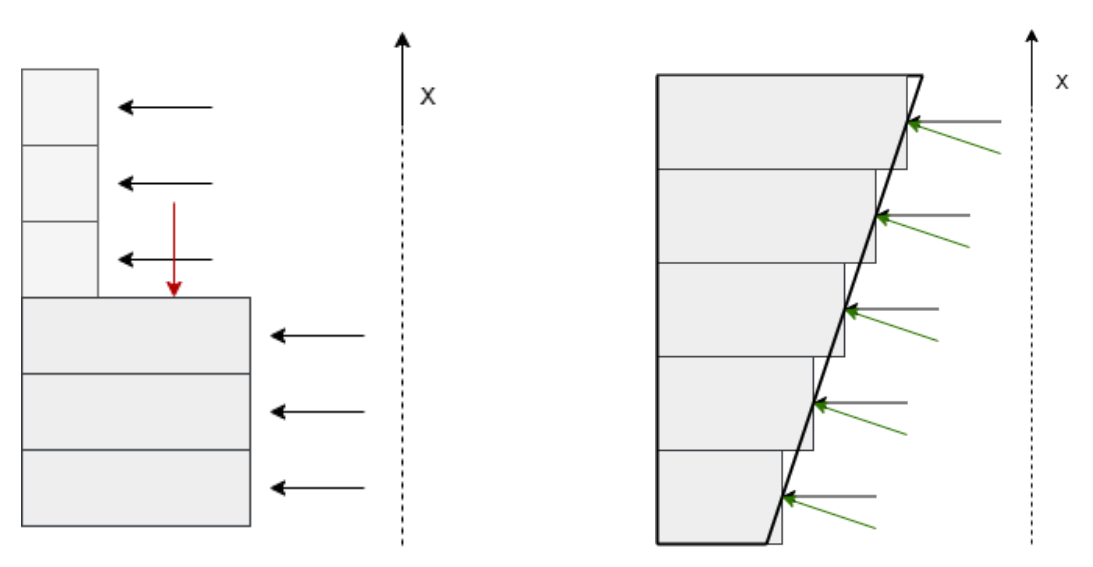


Figure 5 Orientation of regression vector for cylindrical (left) and conical (right) inner grain channel. The red and green arrows depict regression vectors which cannot be modelled by 2D regression models

3. Burn models

The mechanism of combustion in hybrid rocket engine differentiates itself from combustion in solid rocket motors and liquid rocket engines. In solid propellant motors, the combustion takes place on the surface of the grain, as both the oxidiser and the fuel are mixed together in volume of the propellant grain and start to vaporize from the heat provided during ignition. Figure 6 contains a diagram of regions forming during solid propellant grain regression.

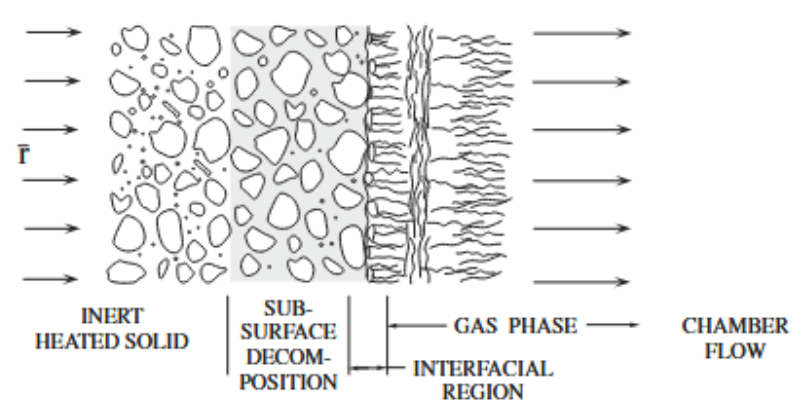


Figure 6 Regions forming during solid propellant combustion [10]

The generally accepted regression rate model uses Saint Robert equation presented in (8), which ties together the regression rate \dot{r} with combustion chamber pressure p_{ch} [11]. Proportionality coefficient a and exponent n of this equation are fitted basing on results of propellant test firings.

$$\dot{r} = a p_{ch}^n \tag{8}$$

An additional phenomenon, which occurs in solid propellant combustion is erosive burn of the propellant. Turbulent flow through the grain channel causes increase in convective heat transfer coefficient thus increasing heat flux accelerating the combustion further the grain length. The impact of erosive burning on total propellant regression rate depends on propellant composition and grain channel dimensions [11].

In hybrid rocket engines, where the oxidiser is fluid and the fuel is stored in solid form, the combustion occurs in the turbulent boundary layer built near the surface of the grain, exposed to the oxidiser flow [12]. In this region the products of grain gasification mix with oxidiser and combust. The heat generated in the combustion process is transferred by

radiation and convection to the grain surface, thus providing the necessary energy for the gasification reaction (see Figure 7). Therefore the regression rate is controlled by the flow conditions and heat transfer, with the latter being the main rate-limiting factor [13].

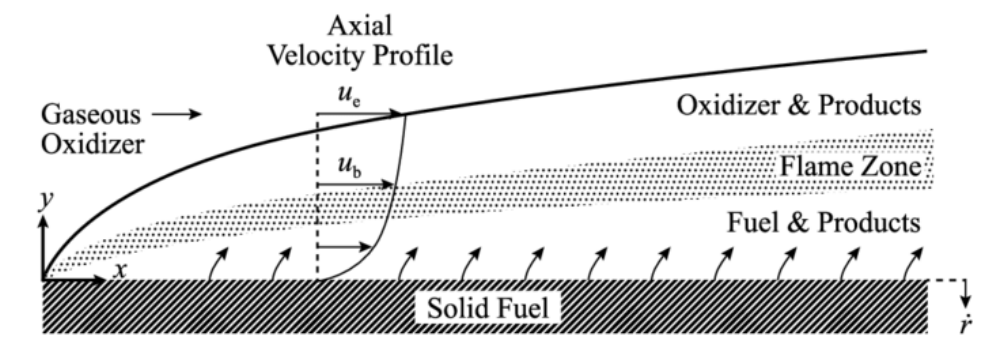


Figure 7 Scheme of combustion process in hybrid rocket motors [14]

The complex nature of this process, involving mechanisms from different fields of physics and chemistry poses challenge in mathematical modelling of the regression rate. The design configuration of the injector, the grain shape and specific propellants choice also contribute to the regression rate characteristics [15-16], therefore creating a fully versatile model of regression rate seems to be impossible. In the following sections of this chapter, a literature review of works devoted to solid fuel burn laws is presented, beginning with early research, which forms the foundations of currently used models.

3.1 Bartel Rannie model

One of the first works, which can be applied to fuel regression rate in hybrid rocket engines was done by Bartel and Rannie [17], who obtained the expression for fuel regression rate presented in equation (9). It was based on assumptions, that the mass flow of fuel has negligible impact on boundary layer and that the fuel and oxidiser mix homogenously.

$$\rho_f \dot{r} = \frac{1}{2} c_f G f_m \exp\left(-\frac{2c_f x}{D}\right) \tag{9}$$

Where G is the total mass flux through the grain channel, f_m is the oxidiser to fuel ratio, x is the position along axis, D is the inner diameter and c_f is the friction coefficient between boundary layer gases and the grain surface, for which Bartel and Rannie used the correlation with Reynolds number [17] presented in equation (10). Here μ is dynamic viscosity of oxidiser.

$$c_f = 0.046Re_D^{-0.2} = 0.046 \left(\frac{GD}{\mu}\right)^{-0.2} \tag{10}$$

Bartel and Rannie model suggests, that the regression rate should reduce exponentially with distance from the injector along the grain axis, while the results of the experiment have shown, that the change of regression rate is not consistent along the chamber length, which will be described in more detail later in the text. Nonetheless, this model was the first to include the $G^{0.8}$ dependency of regression rate, found also in other models, most notably the Marxman-Gilbert model [16].

3.2 Emmons model

Although Emmons's work [18] did not concern combustion in hybrid rocket motors, his research on boundary layer combustion over a solid fuel surface was a significant step in modelling solid fuel grain regression [16]. The model is based on solution of energy, species and momentum conservation laws in steady boundary layer with assumed laminar flame zone [18]. Obtained solution is presented in equation (11).

$$\rho_f \dot{r} = \frac{GY(B)}{\sqrt{Re_x}} \tag{11}$$

Where Re_x is Reynolds number in respect to axial position, Y(B) is a function of heat ratio, defined as thermal energy of unit mass of the main stream relative to the surface, to thermal energy required at the surface to put an unit mass of fuel into the boundary layer [18]. Even though, the assumption of laminar flame nature fails in hybrid rocket engine, where the boundary layer is turbulent, the Emmons's work is important, due to inclusion of the heat ratio, also called the blowing number, found to be relevant for fuel regression rate in later research [16].

3.3 Houser Peck model

Research conducted by Houser and Peck on quasi-real-time regression rate of hybrid fuel grains, measured by the interrupted burning method [19], provided a formula for grain inner radius as function of time:

$$r(t) = A + Bt^{0.8} + Ct^{0.3} (12)$$

Differentiating equation (13) gives power-law formula for regression rate at given time:

$$\dot{r}(t) = 0.8Bt^{-0.2} + 0.3Ct^{-0.7} \tag{13}$$

Where the constants A, B, C are specified empirically. The equation (13) gives highly inaccurate results at time close to zero and does not apply at zero. However, Houser and Peck proved, that the regression rate decreases with engine operation time and increases with the axial distance along the grain [16].

3.4 Saint Robert analogy model

The simplest model of regression rate is presented in equation (14). Parameter G_{ox} is called the oxidiser mass flux and is equal to mass flow rate of oxidiser divided by the combustion port area. The coefficients a and n are obtained by fitting the experiment data for a combination of fuel and oxidiser [15].

$$\dot{r} = aG_{ox}^n \tag{14}$$

This formula yields close resemblance to Saint Robert's formula for regression rate of solid propellants [11], with the chamber pressure replaced by mass flux of oxidiser. This model can be utilized at an early design phase of an engine, basing on the data presented in the literature (chapter 3.7 deals with this topic in greater detail). It should be noted, that fitted curve coefficients depend on the grain channel port and thus may change with variation of the grain geometry.

3.5 Humble's model

Experimental research on hybrid rocket engines regression rate show that the results vary from previously given model with increasing axial position x from the injector. As obtained by Chiaverini et al. [20] the regression rate firstly decreases with x until reaching a global minimum, beyond which it rises further with x. This phenomenon can be explained by two different effects interfering with each other. Along the grain, the thickness of fuel-rich zone in the boundary layer grows, which causes the convective heat flux to decrease in this region. On the other hand, the increase of mass flux in the free stream, caused by injection of fuel into the flow, causes higher convective heat flux. The point of minimum regression rate is the axial location, beyond which the increase in mass flux has greater effect on the regression rate than the increase in boundary layer thickness [16].

Model proposed by Humble et al. [21] includes the above explained effect by modifying the formula presented in (14), multiplying it by axial position factor raised to the power of m (see equation (15)) which value is a result of data fitting. This model is consistent with model presented by Marxman and Gilbert [22], although the exponential coefficients differ from the ones presented in their work, as they are obtained experimentally, not analytically.

$$\dot{r} = \alpha G_{ox}^n x^m \tag{15}$$

3.6 Marxman-Gilbert model

Model developed by Marxman, Gilbert and Woolridge is to this day found to be the milestone for solid fuel burn laws in hybrid rocket engines. They assumed that the combustion occurs in turbulent boundary layer, exactly in a zone separated from one side with fuel rich zone from the grain and with oxidiser rich zone from the combustion chamber flow. In the combustion zone, the concentrations of fuel and oxidiser are not stoichiometric, but sufficient for the combustion reaction to occur [22]. Assuming that the entire heat flux at the fuel surface is dedicated to heating and vaporising a mass unit of fuel, the formula (16) is established [22]:

$$\rho_f \dot{r} = CGRe_x^{-0.2} (St/St_o) (u_e/u_{fl}) [(h_{fl} - h_w)/\Delta H_{v,eff}] + \sigma \varepsilon_w (\varepsilon_g T_{fl}^4 - \alpha_g T_w^4)/\Delta H_{v,eff}$$
 (16)

In equation (16) C is the function of channel flow Mach number, St is the Stanton number of the flow, St_o is the Stanton number in absence of blowing for turbulent flow over a flat plate, u_e is the gas velocity at the boundary layer edge, u_{fl} is the gas velocity in the combustion zone, h_{fl} is the stagnation specific enthalpy at flame temperature, h_w is the specific enthalpy at wall, $\Delta H_{v,eff}$ is the total heat of gasification. Second term of the equation expresses radiant heat transfer, where σ is Stefan – Boltzmann constant, ε_w is emissivity of the wall at flame temperature T_{fl} , and ε_g and α_g are the emissivity and the absorptivity of the gas at the wall temperature T_w . In further work Marxman et al. [12] have shown methods to calculate the factors unknown before engine static fire test. Using the formulas presented in [12], and omitting the radiant heat transfer term (which can be done in particular if the fuel contains no metallic particles or soot [16]), yields a simplified equation for regression rate:

$$\rho_f \dot{r} = 0.0111172 \cdot B^{0.23} Re_x^{-0.2} \frac{kg}{m^2 s} \tag{17}$$

The B parameter is the introduced by Emmons blowing number, for which Marxman defined formula presented in equation (18) [12]. This parameter has two interpretations. From the thermodynamical point of view it describes the ratio of thermal energy of unit mass of combustion products in the main channel flow to energy required to vaporize a unit mass of fuel into the boundary layer [18]. However, it can be also interpreted as parameter of similarity for a boundary layer [12], meaning that if the blowing number is constant along grain axis, and thermal diffusivity is equal to mass diffusivity, the velocity, concentration and enthalpy profiles along the boundary layer thickness are similar inside the entire turbulent boundary layer [16].

$$B = \frac{\rho_w v_w}{\rho_e u_e (c_f/2)} = \frac{u_e}{u_{fl}} \frac{h_{fl} - h_w}{\Delta H_{v,eff}}$$
(18)

Where ρ_w is the density of gases inside the wall boundary layer, v_w is the kinematic viscosity of the gases inside the wall boundary layer, and ρ_e is the free stream density of combustion gases. From the presented models, the Marxman model is the most detailed, taking into considerations many of the factors, which influence the regression rate. Data obtained from experiments have proven that functional form presented in equation (17) is valid, although predicted averaged mass flux is overestimated, and the assumed axial dependence is too high. This can be explained, by the fact that the Marxman model was developed for a grain with slab geometry, while most of currently developed engines utilize grains with either single or multiple internal ports [23].

In this study, two models were selected for the validation with test results: the Saint Robert analogy model and Marxman-Gilbert model without radiation component. Each of them has been successfully implemented in the RPAT programme.

3.7 Overview of burn law coefficients for common combinations of propellants

The following table contains an overview of the Saint Robert analogy model coefficients (see equation (14)) for a set of common propellants. Selected oxidisers were liquid oxygen (LOX), gaseous oxygen (GOX), nitrous oxide (N_2O) and hydrogen peroxide (H_2O_2), whereas considered fuels were hydroxyl-terminated polybutadiene (HTPB), high density polyethylene (HDPE), paraffin, acrylonitrile butadiene styrene (ABS), polymethyl methacrylate (PMMA) and polyethylene (PE) wax. As mentioned earlier, the results of a study are highly dependent on test conditions, therefore observations may differ between the presented and the other studies not included in the table.

	Oxidiser	Fuel	<i>a</i> *	n	G_{ox}	Reference
1	LOX	НТРВ	0.146	0.681	-	[24]
2	LOX	HDPE	0.098	0.620	-	[24]
3	LOX	paraffin	0.488	0.620	-	[24]
4	GOX	HTPB	0.144	0.686	-	[24]
5	GOX	HDPE	0.132	0.498	7.7-26.1	[23]
6	GOX	paraffin	0.488	0.620	1.6-36.9	[23]
7	GOX	PE wax	0.188	0.781	4.8-15.8	[23]
8^{ab}	GOX	ABS	0.480	0.460	1-40	[24]
9	GOX	PMMA	0.087	0.615	3.3-26.6	[23]
10^{a}	N_2O	HTPB	0.417	0.347	5-22	[25]
11 ^a	N_2O	HDPE	0.248	0.331	3-27	[25]
12	N_2O	paraffin	0.491	0.500	-	[24]
13	N_2O	ABS	0.584	0.272	-	[26]
14ª	N_2O	PMMA	0.284	0.335	3-30	[25]
15	H_2O_2	HDPE	0.145	0.529	-	[1]
16	H_2O_2	paraffin	0.490	0.500	-	[27]
17ª	H_2O_2	ABS	0.237	0.595	2.7-9.4	[28]

Table 1 Regression rate model coefficients obtained from selected studies

4. Test bench description

Aurora is an O-class hybrid rocket engine [29] with design performance of 40 kNs of total impulse and 8 kN of maximal thrust. Whole propulsion system consists of liquid oxidiser tank, oxidiser feeding system and combustion chamber. Oxidiser tank is made of aluminium alloy and contains self-pressurized N₂O. On the top side of the tank there is a venting system including solenoid valve, which enables air from the tank to escape while tanking. The tank is connected to the main valve through one-inch braided hydraulic hose. Pyrotechnic in-house designed main oxidiser valve enables a rapid single opening and closing. Combustion chamber consists of composite, carbon fiber reinforced composite body in which paper-phenolic ablative insulation, nozzle and chamber plug are inserted. Chamber plug contains injection plate and igniter assembly. Igniter body allows to place solid (potassium sugar) igniter, later ignition system was upgraded with 3 m of visco fuse glued to the front face of fuel grain. This new igniter configuration was used during the static fire test mentioned later in this chapter. The injection plate is interchangeable with two versions: showerhead and swirl injector. Both injection plates were previously cold flow tested [30]. Cross section through combustion chamber assembly is presented in Figure 8.

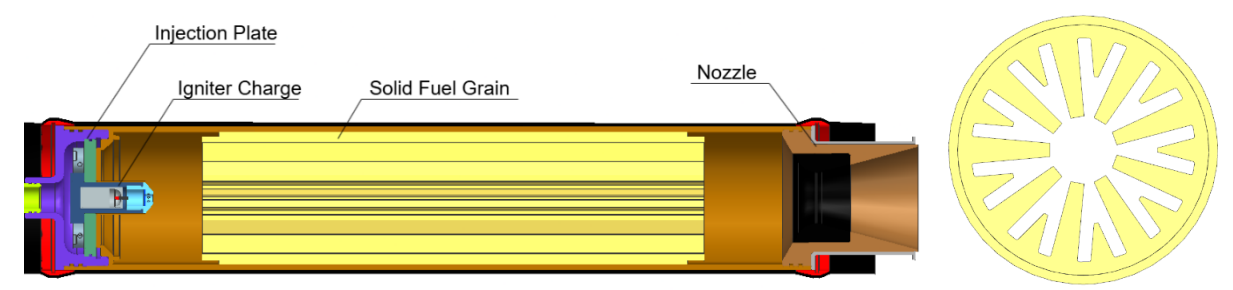


Figure 8 A cross sectional view of Aurora engine combustion chamber assembly (left) and fuel grain geometry (right)

Test bench for current configuration consists of several systems: tanking, pressurisation, feeding and ignition, which together operate each of the engine functions. Starting with the tanking system, its main task is to transport the oxidiser

^{*}Obtained for use with regression rate \dot{r} and oxidiser mass flux G_{ox} in units of respectively $\frac{mm}{s}$ and $\frac{g}{cm^2 s}$

^aG_{ox} range estimated using plots presented in a reference article

^bSelected for a diameter closest to that of the Aurora engine

from industrial nitrous oxide bottles, 5 in total to the engine main oxidiser tank. To provide pressure difference, necessary for tanking, self pressurizing properties of N_2O are employed. Oxidiser stored in bottles is heated by layer of heating foil wrapped around the vessels, which proved to be a reliable solution in previous work [31]. Mass of each bottle as well as the oxidiser tank itself is measured in real time, with reading frequency of $10 \, \text{Hz}$. The flow is initiated through electrical valve linking both vessels. Pressure is measured in real time in the tanking system and in the main tank, with measurement point on one of its ends, worth noting is redundant pressure reading with cameras looking at manometers in hydraulic system. Filling operation is regulated through venting valve, which allows for the pressure release inside the oxidiser tank. Upon reaching the predetermined oxidiser mass inside the tank, the line is cut-off from the bottles with the remotely disconnecting quick-coupler system. From there on, pressure inside the tank is raised with usage of another heating blanket. The simplified scheme of the described test stand is provided in Figure 9.

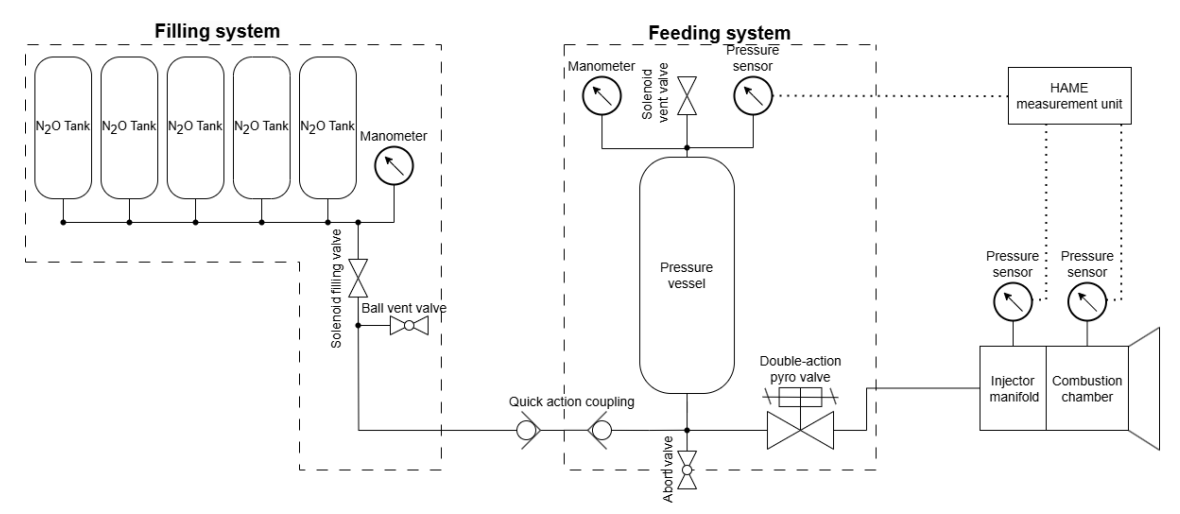


Figure 9 Hot fire test bench setup

Having reached predetermined value of oxidiser pressure, the flow to combustion chamber is initiated through pyrovalve operated remotely with a delay of approximately 2 seconds after igniter charge activation to allow fuel vaporization. In combustion chamber assembly there are two points at which pressure is measured during engine static operation. Those being pressure on the injection plate and in the combustion chamber itself. Both measurements are conducted using Baumer pressure transducers [32] with measurement range of 160 bar and measurement error of maximum 0.5% of the total pressure range. Thrust produced by the motor is measured using WIKA F1821 [33] compression force transducer with measurement range of 10 kN and error of up to 0.5% of the total range.

Main consideration in this work is given to combustion chamber pressure and thrust measurements during the engine operation. Both these measurements are aggregated by the in-house developed HAME measurement unit, which collects live data obtained from measurements at the test stand during firing and enables data recording. As it is presented in the Figure 10, raw data obtained from measurements was significantly noisy and for this reason a moving average algorithm was used to filter the results.

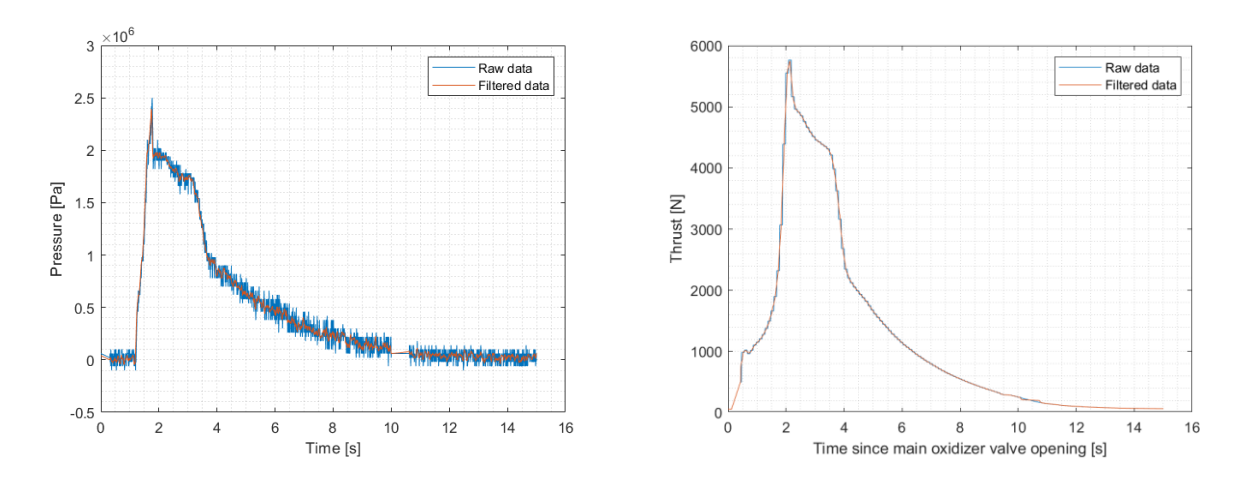


Figure 10 Pressure and thrust curves recorded during test - before and after filtration.

The beginning of measurement curves presented in the Figure 10 corresponds to the moment when the main oxidiser valve is opened. A significant ignition delay (about 2 s) is visible on both presented plots. It should be noted, that during the time required to achieve full engine ignition, the oxidiser is continuously fed into the chamber, which reduces the amount of oxidiser used during nominal engine operation. In addition, the initial amount of oxidiser in the tank was lower than the nominal amount specified at the engine design stage (10.1 kg instead of planned 16 kg). It was caused by insufficient venting valve parameters, which made filling of the tank a very time-consuming process.

5. Validation of burn models

This chapter presents a validation approach based on two of the solid fuel burn rate models mentioned in Chapter 3. These discussions will allow to determine the applicability of the simplest burn rate model based on experimental results (described in Chapters 3.4). Additionally, they will allow to determine the procedure for using burn rate model based solely on physical quantities (as in the case of Marxman model introduced in Chapter 3.6). It is worth noting that from a design perspective, the use of the latter is much more valuable, as it allows the burn rate to be determined without the need for preliminary engine test firings. The validation process itself involved comparing combustion chamber pressure curves obtained during engine simulations in the RPAT programme with experimental data obtained from the test mentioned in Chapter 5. In case of models based on experimental data, selecting the appropriate model coefficients' values required a series of simulations assuming their successively changing values.

It should be noted that a significant obstacle in the process will be the long ignition delay time in relation to the total engine operating time. Based on the available data, it is difficult to determine what the fuel combustion process looked like during this time. However, given the low thrust observed during the ignition delay, it can be assumed that the mass flow rate of fuel during this process was insignificant and that the thrust was generated mainly by the sustained thermal decomposition of the oxidiser. Consequently, it was assumed that the grain geometry did not undergo any regression during the ignition delay. Additionally, the initial conditions for simulations of Aurora engine operation were fitted for the predicted conditions at the moment of achieving full ignition. This concerns mainly the initial oxidiser mass and oxidiser pressure, which values were determined basing on the stand-alone simulation of tank emptying in a way similar to one described in [30]. In this way, the oxidiser mass left in the tank at the moment of ignition was set as 6.7 kg and its pressure at that moment was determined as 45 bar.

Additionally, it should be mentioned that the pressure level achieved in the combustion chamber was significantly lower than that predicted by engine simulations based on thermodynamic parameters obtained in the NASA CEA programme. Since no significant erosion of the combustion chamber nozzle or any additional leakage of combustion products was observed, it can be assumed that the propellants supplied to the combustion chamber volume were not completely burned before they exited through the nozzle. Most likely, the combustion process took place in a mixture with a low oxidiser content (i.e. the local O/F ratio was low). As can be seen on Figure 1, deviating too far from the optimal O/F value (optimal in terms of c^* value) can lead to a significant drop in performance, which was probably observed during this test. This effect introduces an additional difficulty in the implementation of the aforementioned burn law model validation process, as the RPAT programme does not take into account the effects related to combustion efficiency. Therefore, an approach was used whereby the global O/F ratio obtained in each iteration was multiplied by an experimentally fitted coefficient to obtain the local ratio value that occurs in the areas of the chamber where combustion takes place. This value was determined as 0.55 of the global O/F ratio. Value of this experimental coefficient was roughly determined by dividing the total impulse produced during engine operation by the total impulse obtained during motor simulation. It is further assumed that the rest of oxidiser entering the chamber is undergoing thermal decomposition and then the thermal parameters of mixture of decomposed oxidiser and combustion products is considered actual for further calculation of engine performance and, in particular combustion chamber pressure within RPAT programme. In the Table 2 the input parameters describing engine construction for simulations conducted to obtain correlation are summarised.

Table 2 Summary of static fire te	st parameters
-----------------------------------	---------------

Parameter	Value	Unit
Oxidiser mass	10.1	kg
Initial oxidiser pressure (pre-injector)	51.5	bar
Nozzle throat diameter	45	mm
Fuel mass	3.4	kg
Combustion chamber volume	$3.4\cdot 10^{-3}$	m^3
Injector hole diameter	1	mm
Number of injector holes	108	-

During the aforementioned process of matching the experimental pressure curves and those obtained from the simulation using the experimental combustion law model presented in equation (14), the range of combustion law coefficient values from 0.1 to 0.7 mm/s with a step of 0.15 and the range of combustion law exponent values from 0.05 to 0.55 with a step of 0.1 were considered. Engine operation simulations were performed for the resulting grid of 30 calculation points. Final values of coefficients were selected, basing on the slope of the curves, fitting the test data the most.

For the Marxman model implementation a second formulation from equation (18) is used, where specific enthalpy of flame h_{fl} and specific enthalpy of the gasified fuel h_w is computed:

$$h_{fl} = c_{pfl}(T_{fl} - T_0) (19)$$

$$h_w = c_{pw}(T_w - T_0) (20)$$

Where the c_{pfl} is the flame specific heat at constant pressure, c_{pw} is specific heat at constant pressure of the gasified fuel, T_W is fuel vaporisation temperature and T_0 is reference temperature which in this case is set as ambient temperature.

Obtaining the chemical parameter $\frac{h_{fl}-h_w}{\Delta H_{v,eff}}$ allows for obtaining flame position parameter $\frac{u_e}{u_{fl}}$:

$$\frac{u_e}{u_{fl}} = \frac{O/F \frac{h_{fl} - h_w}{\Delta H_{v,eff}}}{K_{Oxe} + (O/F + K_{Oxe}) \left(\frac{h_{fl} - h_w}{\Delta H_{v,eff}}\right)}$$
(21)

Where ${}^{O}/_{F}$ is local oxidiser to fuel ratio and K_{0xe} is a concentration of oxidiser in injected liquid or gaseous mixture (ratio between oxidiser and total injected mass flow including inert additives) and since the pure N₂O was used as an oxidizer, in this case this coefficient is equal to unity. For validation of this model, a simulation was performed using described implementation and the result is presented in Figure 11. Additional variables were added to the programme input and are presented in Table 3.

Table 3 Marxman model variables

Parameter	Value	Unit
Gasified fuel specific heat [34]	1534.24	<u>J</u> kg⋅K
Total heat of gasification ^a [35]	1633	$\frac{J}{kg}$
Fuel vaporisation temperature [36]	697.15	K
Concentration of oxidiser	1	-

^aDue to a lack of information about ABS decomposition products, value corresponding to styrene (dominant ABS component) were assumed

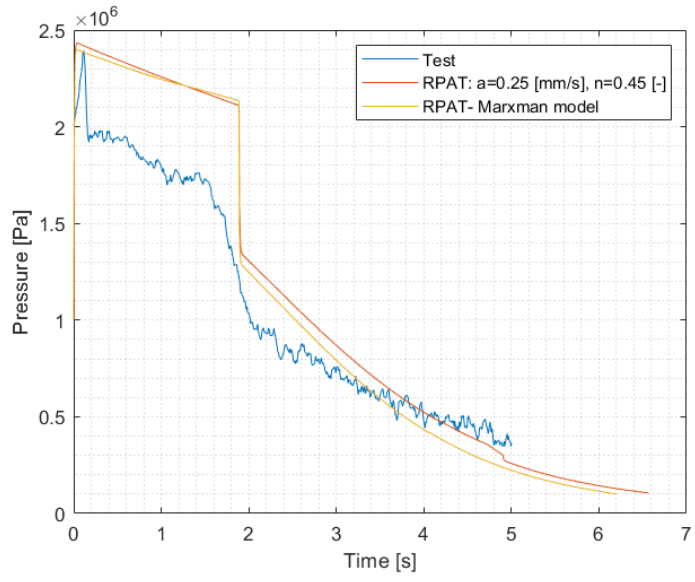


Figure 11 Comparison of pressure curves obtained from simulation using Marxman and Saint Robert analogy burn rate models with experimental pressure curve

Despite the fact, that the physical data regarding combustion products, which was used for the Marxman model setup was partially approximated, the resulting pressure curve is similar to one obtained using former, Saint Robert analogy model. The fact that the curves obtained using both models are similar is promising for the prospect of using the model in the design stage of hybrid engines. This means that the use of the Marxman model can eliminate the uncertainty resulting from the need to adopt experimental values of combustion coefficients, according to a model analogous to Saint Robert's, while accurately reproducing the physical process of fuel combustion. At the same time, the Marxman model requires relatively little physical data on the propellant to be implemented. Both pressure curves obtained from RPAT simulations during validation (see Figure 11) seem to reflect the nature of the test curve in terms of the rate of pressure change in the combustion chamber.

6. Summary

Due to the widely recognised difficulty in determining the combustion speed of fuel grains in a hybrid engine, a wide range of models attempting to replicate this phenomenon have been developed over the years of research into such systems. Despite the fact that some of the models discussed in Chapter 3 have not gained popularity, the overall research conducted to validate them has contributed to the development of models used today. This study validated the most promising of these combustion models to confirm their accuracy. However, the validation was based on hybrid engine operating conditions that were far from standard. The main reason for this is the significant ignition delay, which probably led to unknown and neglected in the conducted analysis changes in fuel grain geometry. In addition, during the validation, it was noted that the actual combustion chamber pressure during engine operation is much lower than that predicted in the simulations. The reason for this is probably incomplete propellant combustion. An additional (albeit minor) reason for the discrepancy between the simulations and the actual results may also be the inaccuracy of the fuel grain geometry mapping in the RPAT programme, which was discussed in Chapter 2.

Acknowledgments

Participation of authors of this paper in EUCASS 2025 was funded by the Polish Ministry of Science and Higher Education as part of the *Wsparcie studentów w zakresie podniesienia ich kompetencji i umiejętności* programme. Development of Aurora hybrid propulsion system was supported by the Ministry of Science and Higher Education as a part of the *Studenckie kola naukowe tworzą innowacje 4.0* programme.

References

[1] A. Okninski *et al.*, 'Development of Green Storable Hybrid Rocket Propulsion Technology Using 98% Hydrogen Peroxide as Oxidizer', *Aerospace*, vol. 8, no. 9, p. 234, Aug. 2021, doi: 10.3390/aerospace8090234.

- [2] D. Pastrone, 'Approaches to Low Fuel Regression Rate in Hybrid Rocket Engines', *Int. J. Aerosp. Eng.*, vol. 2012, pp. 1–12, 2012, doi: 10.1155/2012/649753.
- [3] T. Palacz and J. Cieslik, 'Experimental investigation of the regression rate in an end-burning swirling flow hybrid rocket engine', p. 11 pages, 2022, doi: 10.13009/EUCASS2022-4535.
- [4] M. Calabro, 'Overview on Hybrid Propulsion', Oct. 2012. doi: https://doi.org/10.1051/eucass/201102353.
- [5] S. R. Gomes, L. Rocco Junior, and J. A. F. F. Rocco, 'Swirl Injection Effects on Hybrid Rocket Motors', *J. Aerosp. Technol. Manag.*, vol. 7, no. 4, pp. 418–424, Nov. 2015, doi: 10.5028/jatm.v7i4.368.
- [6] Ch. Glaser, J. Hijlkema, J. Lestrade, and J. Anthoine, 'The Stepped Helix Hybrid Rocket Engine', presented at the AIAA AVIATION 2023 Forum, Jun. 2024. doi: 10.2514/6.2023-4028.
- [7] S. Gordon, 'Computer Program for Calculation of Complex Chemcial Equilibrium Compositions and Applications', 1994.
- [8] M. Tomporowski *et al.*, 'Development and validation of rocket motor simulation software', presented at the 75th International Aeronautical Congress, Oct. 2025. doi: https://doi.org/10.52202/078371-0116.
- [9] J. Dyer, E. Doran, Z. Dunn, K. Lohner, and G. Zilliac, 'Modeling Feed System Flow Physics for Self-Pressurizing Propellants', Jul. 2007, doi: 10.2514/6.2007-5702.
- [10] Multiple, 'Internal Aerodynamics in Solid Rocket Propulsion', NATO, Educational Notes RDP RTO-EN-023, Jan. 2004.
- [11] A. Davenas, *Solid Rocket Propulsion Technology*. Elsevier Science & Technology Books, 1993. [Online]. Available: https://books.google.pl/books?id=UZpTAAAAMAAJ
- [12] G. A. Marxman, C. E. Wooldridge, and R. J. Muzzy, 'Fundamentals of Hybrid Boundary-Layer Combustion', in *Progress in Astronautics and Rocketry*, vol. 15, Elsevier, 1964, pp. 485–522. doi: 10.1016/B978-1-4832-2730-6.50025-7.
- [13] R. J. Muzzy, 'Applied hybrid combustion theory', in 8th Joint Propulsion Specialist Conference, American Institute of Aeronautics and Astronautics. doi: 10.2514/6.1972-1143.
- [14] T. Marquardt and J. Majdalani, 'A Primer on Classical Regression Rate Modeling in Hybrid Rockets', Aug. 2020. doi: 10.2514/6.2020-3758.
- [15] G. Sutton and O. Biblarz, Rocket Propulsion Elements, 7th edition. New York: John Willey & Sons, 2001.
- [16] M. J. Chiaverini and K. K. Kuo, *Fundamentals of Hybrid Rocket Combustion and Propulsion*, vol. 218. in Progres In Aeronautics And Astronautics, vol. 218. American Institute of Aeronautics and Astronautics, Inc., 2007. Accessed: May 08, 2025. [Online]. Available: https://arc.aiaa.org/doi/book/10.2514/4.866876
- [17] H. R. Bartel and W. D. Rannie, 'Solid fuel combustion as applied to ramjets', Pasadena Jet Propuls. Lab., 1946.
- [18] H. W. Emmons, 'The Film Combustion of Liquid Fuel', *ZAMM J. Appl. Math. Mech. Z. Für Angew. Math. Mech.*, vol. 36, no. 1–2, pp. 60–71, 1956, doi: 10.1002/zamm.19560360105.
- [19] T. J. Houser and M. V. Peck, 'Research in Hybrid Combustion', in *Progress in Astronautics and Rocketry*, vol. 15, H. G. Wolfhard, I. Glassman, and L. Green, Eds., in Heterogeneous Combustion, vol. 15., Elsevier, 1964, pp. 559–581. doi: 10.1016/B978-1-4832-2730-6.50027-0.
- [20] M. J. Chiaverini, N. Serin, D. K. Johnson, Y.-C. Lu, K. K. Kuo, and G. A. Risha, 'Regression Rate Behavior of Hybrid Rocket Solid Fuels', *J. Propuls. Power*, vol. 16, no. 1, pp. 125–132, Jan. 2000, doi: 10.2514/2.5541.
- [21] R. Humble, H. Gary, and W. Larson, Space propulsion analysis and design. 1995.
- [22] G. Marxman and M. Gilbert, 'Turbulent boundary layer combustion in the hybrid rocket', *Symp. Int. Combust.*, vol. 9, no. 1, pp. 371–383, Jan. 1963, doi: 10.1016/S0082-0784(63)80046-6.
- [23] G. Zilliac and M. Karabeyoglu, 'Hybrid Rocket Fuel Regression Rate Data and Modeling', in 42nd AIAA/ASME/SAE/ASEE Joint Propulsion Conference & Exhibit, Sacramento, California: American Institute of Aeronautics and Astronautics, Jul. 2006. doi: 10.2514/6.2006-4504.
- [24] S. A. Whitmore and S. Merkley, 'Radiation Heating Effects on Oxidizer-to-Fuel Ratio of Additively Manufactured Hybrid Rocket Fuels', *J. Propuls. Power*, vol. 35, no. 4, pp. 863–878, Jul. 2019, doi: 10.2514/1.B37037.
- [25] E. Doran, J. Dyer, K. Lohner, Z. Dunn, B. Cantwell, and G. Zilliac, 'Nitrous Oxide Hybrid Rocket Motor Fuel Regression Rate Characterization', in 43rd AIAA/ASME/SAE/ASEE Joint Propulsion Conference & Exhibit, American Institute of Aeronautics and Astronautics. doi: 10.2514/6.2007-5352.
- [26] R. Wubben, 'Hydrocarbon Seeded ABS Nitrous Hybrid Engine Development', 2022, Accessed: Jun. 01, 2025. [Online]. Available: https://repository.tudelft.nl/record/uuid:7655afc0-97f1-4653-be26-b6bc5b003523
- [27] E. Toson and A. M. Karabeyoglu, 'Design and Optimization of Hybrid Propulsion Systems for In-Space Application', in 51st AIAA/SAE/ASEE Joint Propulsion Conference, Orlando, FL: American Institute of Aeronautics and Astronautics, Jul. 2015. doi: 10.2514/6.2015-3937.
- [28] S. A. Whitmore, I. W. Armstrong, M. C. Heiner, and C. J. Martinez, 'High-Performing Hydrogen Peroxide Hybrid Rocket with 3-D Printed and Extruded ABS Fuel', in *2018 Joint Propulsion Conference*, Cincinnati, Ohio: American Institute of Aeronautics and Astronautics, Jul. 2018. doi: 10.2514/6.2018-4443.

- [29] 'National Association of Rocketry Rocket Motor Resources National Association of Rocketry'. Accessed: Jun. 07, 2025. [Online]. Available: https://www.nar.org/RocketMotorResources
- [30] M. Dzik, B. Hyży, Sz. Życiński, and P. Łyżwa, 'Swirl Injectors in Hybrid Rocket Engine Design, Parameters Validation and Applicability in a N2O/ABS Hybrid Rocket Booster', presented at the 75th International Aeronautical Congress, doi: 10.52202/078371-0143.
- [31] M. Dzik, B. Hyży, D. Legutko, A. Kwitek, P. Chernenko, and J. Czerniej, 'Course and challenges of flight qualification test campaign of the students' hybrid rocket engine', presented at the 74th International Astronautical Congress (IAC), Baku, 2023.
- [32] 'ds_fo5159_en_co.pdf'. Accessed: Jun. 14, 2025. [Online]. Available: https://www.wika.com/media/Data-sheets/Force/Compression-force-transducers/ds fo5159 en co.pdf
- [33] 'Force sensor / force transducer WIKA'. Accessed: Jun. 14, 2025. [Online]. Available: https://www.wika.com/en-en/lp_force_sensor.WIKA
- [34] Styrene, NIST Chemistry WebBook, SRD 69. Accessed: Jun. 14, 2025. [Online]. Available: https://webbook.nist.gov/cgi/cbook.cgi?ID=C100425&Mask=1#Thermo-Gas
- [35] R. Balart, D. Garcia-Sanoguera, L. Quiles-Carrillo, N. Montanes, and S. Torres-Giner, 'Kinetic Analysis of the Thermal Degradation of Recycled Acrylonitrile-Butadiene-Styrene by non-Isothermal Thermogravimetry', *Polym. 2019*, vol. 11, no. 2, Feb. 2019, doi: https://doi.org/10.3390/polym11020281.
- [36] ABS: Acrylonitrile-Butadiene-Styrene Copolymer. Accessed: Jun. 14, 2025. [Online]. Available: https://polymers.netzsch.com/Materials/Details/1